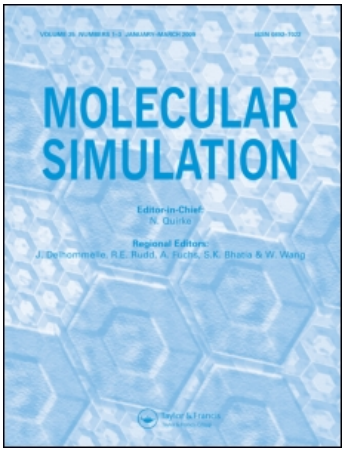

Molecular Simulation
Publication details, including instructions for authors and subscription information:
http://www.informaworld.com/smpp/title~content=t713644482

Selective attachment of monovalent background electrolyte ions and growth inhibitors to polar steps on sulfates as studied by molecular simulations and AFM observations

Udo Becker[a]; Peter Risthaus[b]; Dirk Bosbach[c]; Andrew Putnis[a]
[a] Institut für Mineralogie, Universität Münster, Münster, Germany [b] Forschungszentrum Karlsruhe, Institut für Materialforschung III, Karlsruhe, Germany [c] Forschungszentrum Karlsruhe, Institut für Nukleare Entsorgung, Karlsruhe, Germany

Online publication date: 26 October 2010

To cite this Article Becker, Udo , Risthaus, Peter , Bosbach, Dirk and Putnis, Andrew(2002) 'Selective attachment of monovalent background electrolyte ions and growth inhibitors to polar steps on sulfates as studied by molecular simulations and AFM observations', Molecular Simulation, 28: 6, 607 — 632
To link to this Article: DOI: 10.1080/08927020290030161
URL: http://dx.doi.org/10.1080/08927020290030161

Molecular Simulation, 2002 VOL. 28 (6-7), pp. 607–632

SELECTIVE ATTACHMENT OF MONOVALENT BACKGROUND ELECTROLYTE IONS AND GROWTH INHIBITORS TO POLAR STEPS ON SULFATES AS STUDIED BY MOLECULAR SIMULATIONS AND AFM OBSERVATIONS

UDO BECKER[a,*], PETER RISTHAUS[b], DIRK BOSBACH[c] and ANDREW PUTNIS[a]

[a]*Institut für Mineralogie, Universität Münster, Corrensstraße 24, 48149 Münster, Germany;* [b]*Forschungszentrum Karlsruhe, Institut für Materialforschung III, Postfach 3640, 76021 Karlsruhe, Germany;* [c]*Forschungszentrum Karlsruhe, Institut für Nukleare Entsorgung, Postfach 3640, 76021 Karlsruhe, Germany*

(Received April 2001; In final form August 2001)

Molecular simulations and *in situ* atomic force microscopy (AFM) experiments are used to demonstrate the influence of the ionic strength of the solution and the mechanism of growth inhibitors on growth and dissolution of barite with some comparative experiments on celestite. Growth and dissolution rates, as determined from monolayer step edge velocities, increase with increasing background electrolyte (NaCl) concentration. The electrolyte effect is analyzed in terms of changes of the bulk solution, physicochemical properties of the near-surface region and the mechanisms on the sulfate surfaces at a molecular scale. Bulk solution effects are mainly based on changes in the activity coefficient of dissolved species whereas increased growth and dissolution rates are partly due to a decreased interfacial tension between barite and supersaturated aqueous solution at high ionic strength. We have also found possible mechanisms from molecular simulations that explain the rate changes and also the significant changes in morphologies of etch pits and growth islands when monovalent background electrolyte ions are added. In solutions with high ionic strength, the relative stability of polar [010] steps is increased in comparison to the dipole-free ⟨120⟩ direction, evident as growth islands and etch pits, which are elongated in the [010] direction under growth and dissolution conditions, respectively. This indicates a specific interaction between the background electrolyte and certain sites on the mineral surface. The increased relative stability of steps parallel to [010] relative to those parallel to ⟨120⟩ could be explained by the formation of stabilized $-Na-SO_4-Na-SO_4-$ or $-Cl-Ba-Cl-Ba-Cl-$ chains along the step, which are less polar than terraces bounded by either SO_4^{2-}

*Corresponding author. Tel.: +49-251-8336107. Fax: +49-251-8338397. E-mail: ubecker@uni-muenster.de.

ISSN 0892-7022 © 2002 Taylor & Francis Ltd
DOI: 10.1080/08927020290030161

or Ba^{2+}. The most likely explanation for the increased growth velocity is that Na^{+} ions in solution can attach to preexisting growth islands to start a new growth row, which is the rate limiting step for growth in solutions with a low salinity.

Keywords: Growth inhibitor; Barite; AFM; Background electrolyte

INTRODUCTION

Barite scale is a frequently encountered problem in off-shore exploration because large amounts of seawater are injected into the oil containing reservoir rocks to maintain the inner pressure, which is essential for the efficient extraction of oil. Barite ($BaSO_4$) is a common scale-forming mineral due to its relatively low solubility ($\log K_{sp} = -9.96$ at 20°C [1]) compared to other typical scale minerals such as calcite ($\log K_{sp} = -8.48$ at 25°C [2]) and celestite ($\log K_{sp} = -6.62$ [3]). The high concentration of sulfate ions in the injected seawater (28.1 mM [4]) and the concentration of alkaline earth elements (including Ba^{2+}) in the formation water of 0.07–18.2 mM [4] causes a highly supersaturated solution with respect to barite if these fluids are mixed. As a result, barite precipitates may form in the pipes in the production well and also reduce the porosity of the reservoir [5].

Various strategies are pursued to solve the scale problem: (i) crystal growth inhibitors are used to prevent scale precipitation. The attachment of these organic molecules to active growth sites disrupts the nucleation process and hinders the continuation of growth. (ii) complexing agents are applied to dissolve barite precipitates. This has the disadvantage that large amounts of chelators are necessary because one chelator molecule is consumed for each dissolved cation.

In order to understand barite scale formation and to improve scale treatment technologies, a sound understanding of the complex precipitation and dissolution processes is required. Although much work has been dedicated to study these processes from a macroscopic point of view [6], the microscopic mechanisms such as two-dimensional nucleation, spiral growth or etch pit formation have to be studied at a molecular level. Atomic force microscopy (AFM) can be used to characterize individual growth and dissolution mechanisms *in situ*. Details on barite growth and dissolution have been reported in numerous AFM studies [7–11]. Special attention has been paid to the effect of organic growth inhibitors [12–14], organic chelators [13,15], pH [16,17] and temperature [11,18,19]. However, at this point, the influence of the ionic strength on the barite scale formation has been neglected in microscopic studies, although in off-shore exploration, the injected seawater has high ionic strength ($I = 0.7$). Only one study for calcite has attempted this: Shiraki *et al.* [20] have determined the dissolution kinetics in 0.1 M NaCl solution in AFM experiments.

Macroscopic experiments indicate that barite precipitation [21] and dissolution kinetics are affected by the presence of background electrolytes [1,3,22]. Here, we present AFM observations on the influence of the ionic strength on growth and dissolution of barite with some comparative experiments with celestite. Furthermore, certain microtopographic features such as the morphology of etch pits and molecular islands can be clearly associated with the presence of specific background electrolytes. In highly saline solutions, we obtain very similar etch pit morphologies to those which have been previously attributed to specific interactions between organic molecules and certain sites on a mineral surface [17,23].

In recent years, an increasing number of molecular simulation studies were performed on the influence of foreign cations and inhibitor molecules on the growth and dissolution of mineral surfaces, in particular on carbonate (e.g. [24–29]) and sulfate surfaces [30–34]. It was shown that a precise description of hydration energies in solution and at the surface is crucial for the analysis of the subtle but significant differences of the adsorption thermodynamics of different ions on specific surface sites [34,35]. The net adsorption energy to a specific surface site can be decomposed into three different energy contributions, which are the hydration energy in bulk water (which tends to prevent adsorption), the adsorption energy in vacuum, and the partial hydration energy on the surface (the latter two promote adsorption). Each of these relatively large energy contributions needs to be evaluated precisely to obtain a sensible value for the relatively small remaining net adsorption energy. It can be a formidable task to derive all these energy contributions for all relevant surface sites (mineral, face, step, kink, and adsorbate dependent) but this knowledge will be necessary to predict thermodynamic equilibria of the adsorption of different cations or to judge if growth inhibitor molecules will be overgrown or re-dissolved ([25,36]). The aim of this study is to use the combination of AFM results from experiments in a fluid cell and of molecular simulations to identify the rate limiting steps for growth and dissolution under different solution conditions. Subsequently, it is possible to describe the role of adsorption and hydration to explain the mechanisms and reaction pathways that a surface undergoes depending on the composition of a solution in contact with a specific mineral surface.

EXPERIMENTAL METHODS

Observations of crystal growth and dissolution were made in a fluid cell of a Digital Instruments NanoScope III Multimode AFM, working in contact mode at room temperature. The analyzed minerals, barite, and celestite were optically

clear natural crystals, freshly cleaved parallel to the cleavage plane (001). The crystallographic orientation of the sample crystals with respect to the AFM scan direction was determined from the observed etch pit morphology [13,37].

Nucleation and dissolution experiments in the fluid cell were performed in free drift experiments. After the injection of the solutions into the fluid cell, the fluid flow was stopped while the images of the growth or dissolution experiment were recorded. As a consequence, the fluid composition changed as crystal growth or dissolution continued. However, the velocities of advancing molecular steps were measured immediately after the fluid injection, at which point, the influence of changes in the solution composition could be neglected.

Supersaturated $BaSO_4$ and $SrSO_4$ solutions were prepared by mixing equimolar Na_2SO_4 and $Ba(NO_3)_2$/$Sr(NO_3)_2$ solutions made of analytical grade chemicals and deionized water immediately before the experiment. The degree of supersaturation and the ionic strength were determined using the aqueous speciation code PHREEQC [38]. Throughout this paper, the supersaturation will be expressed as $S = \mathrm{IAP}/K_{\mathrm{sp}}$, where IAP is the ion activity product of the ionic species in solution and K_{sp} is the solubility product of the growing mineral ($\log K_{\mathrm{sp}}(\mathrm{barite}) = -9.96$ [1] and $\log K_{\mathrm{sp}}(\mathrm{celestite}) = -6.62$ [3]).

More details on the experimental conditions can be found in Ref. [30].

COMPUTATIONAL METHODS

Calculations of sulfate surfaces and on the interaction between background electrolyte ions and specific surface features were performed using empirical potential force field models based on the sulfate potentials developed by Ref. [31]. For all computations of step and adsorption energies, we applied two-dimensional periodic boundary conditions parallel to the surface. For computations involving surface relaxation, the two uppermost molecular layers were allowed to relax. This was tested to be sufficient because on sulfate surfaces, relaxation perpendicular to the surface predominantly takes place in these two layers in addition to tilts and rotations of surface sulfate molecules.

Step energies, which we define as the energies that a surface step is energetically less favorable (per unit length of step) than the same number of atoms on a flat terrace are calculated by comparing a relaxed step structure with a relaxed flat surface ("relaxed" case) or an unrelaxed step with a bulk terminated surface ("unrelaxed" case).

Hydration energies of ions dissolved in solution were taken from experimental values from Ref. [39] and references therein. Hydration energies of adsorbed surface species were calculated by performing molecular dynamics simulations

with four water layers on the surface with, and without the adsorbed species (see also Ref. [40]). Water potentials were tested to be in good agreement (less than 5% error) with the experimental hydration energies by applying the droplet method described in Ref. [39].

The adsorption of H_2-$HEDP^{2-}$ as a typical growth inhibitor molecule was analyzed. H_2-$HEDP^{2-}$ was used because this is the protonation state at neutral pH values and H_2-$HEDP^{2-}$ has the same charge as SO_4^{2-}. Therefore, adsorption energies of the two anions can be easily compared. Potentials used to calculate the adsorption and hydration energies of H_2-$HEDP^{2-}$ to $BaSO_4$ steps were derived using the optimized structures (some of which are shown in Fig. 1) and binding energies from quantum mechanical calculations. We used the program package GAUSSIAN98 [41] for these calculations, with a hybrid method of the Hartree–Fock (HF)/Density Functional Theory (DFT), the so-called Becke3LYP

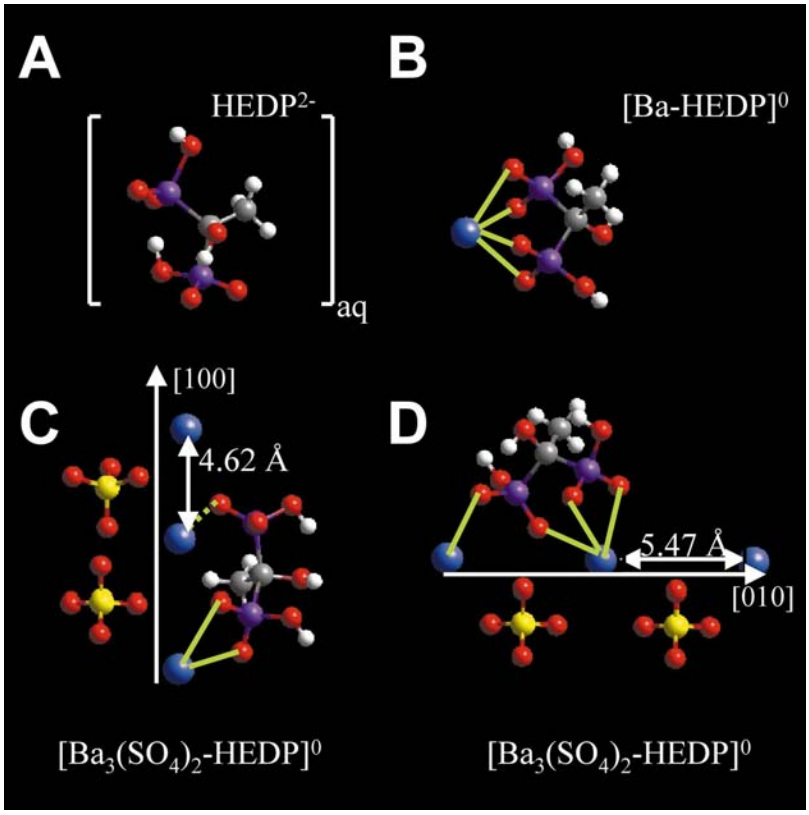

FIGURE 1 H_2-HEDP-fragments used in quantum mechanical calculations (GAUSSIAN98) to derive force field potentials.

approach. The basis sets applied were Pople-type 6-31g* basis sets on all smaller atoms, and a LANL2DZ pseudopotential basis set on Ba. Hydration energies of HEDP molecules were calculated with the polarized continuum model (PCM) [42]. In the quantum mechanical runs with the fragment of a step and the H_2-$HEDP^{2-}$ adsorbed to it, the H_2-$HEDP^{2-}$ was allowed to relax but the fragment of the step was kept rigid (Fig. 1C and D) in order to model the characteristic step structure and atomic distances better. The potentials were refined using the CVFF potentials as a basis ([43], see also Ref. [33]) and then incorporating the results from the quantum mechanical runs (structures and energies) in the potential fitting procedure incorporated in the program package GULP [44]. Potentials were then transferred to Cerius[2] and used for the calculation of the structure and adsorption energies of more complex structures.

EXPERIMENTAL RESULTS

Crystal Growth: Monolayer Step Growth

The most dominant growth mechanism on barite and celestite surfaces is the attachment of ions from solution onto kink sites leading to the advancement of molecular steps. The growth kinetics of such steps was studied at various background electrolyte concentrations. However, in order to study this effect quantitatively, step growth rates were measured on barite (001) surfaces at

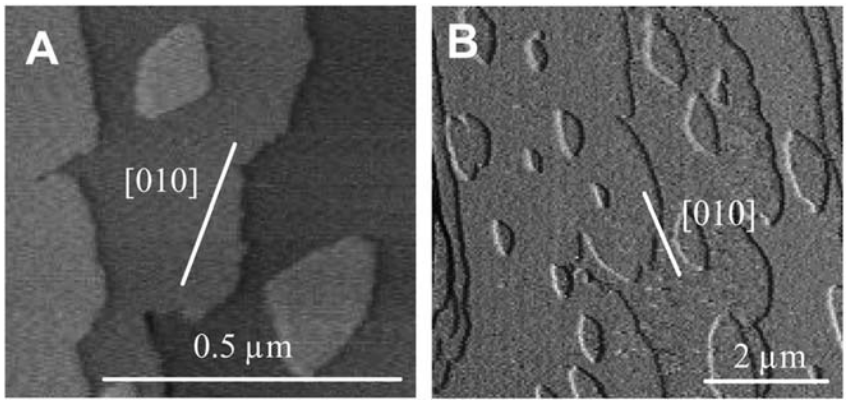

FIGURE 2 (A) Two-dimensional nuclei are formed on the (001) surface in a supersaturated pure $BaSO_4$ solution. Note the opposite orientation of the sector-shaped islands in consecutive layers. (B) For the same supersaturation, the islands become more elongated with increasing NaCl content (increasing ionic strength, 0.75 here).

constant supersaturation with increasing ionic strength. Due to the decrease of the mean activity coefficients of aqueous Ba^{2+} and SO_4^{2-}, the concentration of Ba^{2+} and SO_4^{2-} in solution had to be increased with increasing salinity. In addition, the formation of $NaSO_4^-$ and $BaSO_4$ species in solution reduces the free SO_4^{2-} activity further. Consequently, the Ba^{2+} and SO_4^{2-} concentrations have to be increased non-stoichiometrically with increasing NaCl background electrolyte concentration.

After injecting a moderately supersaturated $BaSO_4$ solution ($S = 19.6$) with low background electrolyte concentration (ionic strength $= 0.003$) into the AFM fluid cell, two-dimensional islands with a height of one molecular $BaSO_4$ layer form on a barite (001) surface as shown in Fig. 2A. Their lateral spreading results in a distinct circular sector-shaped morphology, which reflects the relative growth rates in different crystallographic directions. The morphology is controlled by straight step edges parallel to [120] and [1$\bar{2}$0] and a curved step edge between them. The orientation of these islands alternates in consecutive molecular layers due to the 2_1 screw axis parallel to [001]. Following the PBC theory [45,9], step edges parallel to ⟨120⟩ are related to a sequence of straight bonds resulting in a low kink site density. On the other hand, the curved step edges necessarily have a high kink site density. Therefore, the curved step edges are the most reactive parts of the barite (001) surface where step growth preferentially occurs [13]. The

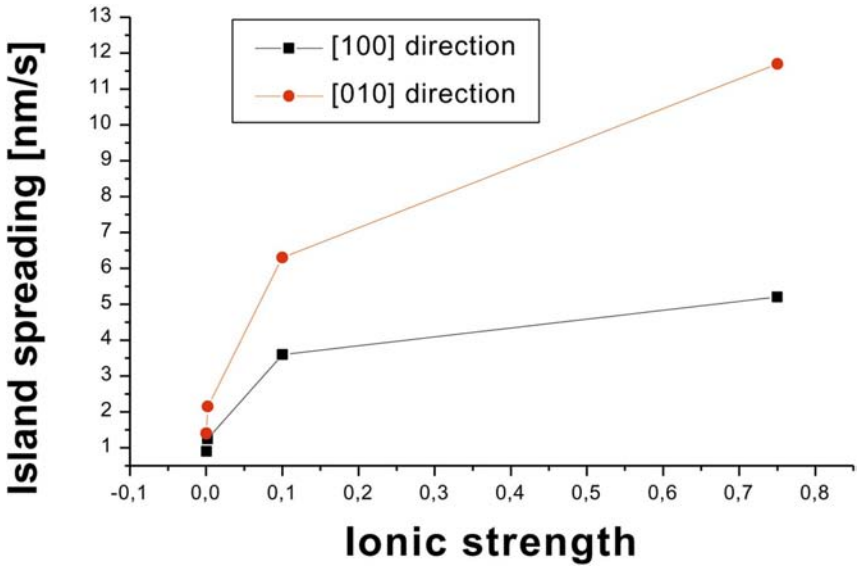

FIGURE 3 Island spreading velocity vs. ionic strength with constant supersaturation ratio.

growth velocity of these islands is highly anisotropic. Growth normal to the curved step edges is approximately 10 times faster than growth normal to the straight edges.

Figures 2A, B and 3 indicate that the monolayer step velocity increases with increasing ionic strength at constant supersaturation. However, monolayer step growth is not increased by the same factor for all crystallographic directions. Therefore, the island morphology and aspect ratio changes depending on the background electrolyte concentration. Molecular islands are more elongated in the [010] direction and the angle between the straight edges (originally [120] and $[1\bar{2}0]$) of the sector-shaped islands become more obtuse. At very high ionic strength (Fig. 2B), it becomes difficult to distinguish between the straight step edges and the curved ones relative to the original sector-shaped islands. Only the tangents at the corners of the islands and thus, the starting points of the growth rows, may be parallel to the original ⟨120⟩ PBC directions. The ratio of the mean growth velocities of [010] and [100] directions causes the elongation of the islands (Fig. 3).

The formation of growth spirals is also affected by the relative changes in monolayer step edge reactivity with increasing ionic strength. The contribution of spiral growth on the barite (001) surface to the overall volume growth is limited by the slowest step advancements because spirals are bounded by these steps [10]. On barite (001) surfaces, these bounding steps are parallel to ⟨120⟩ at low ionic strength (Fig. 4A). This leads to spiral growth hillocks with relatively little lateral

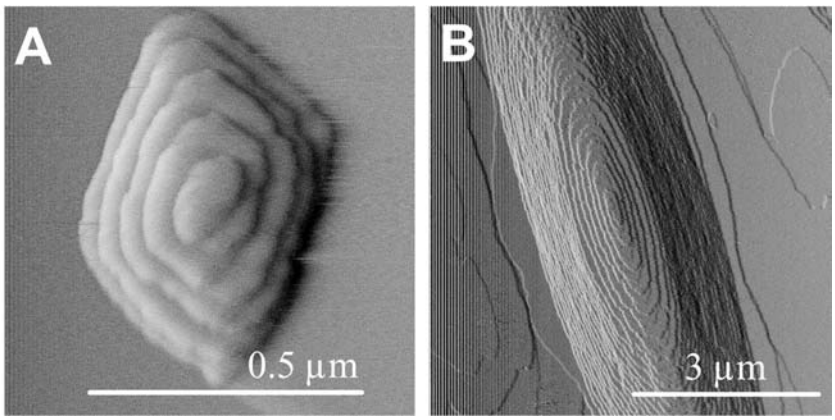

FIGURE 4 (A) Due to the growth anisotropy in consecutive $BaSO_4$ layers, the shape and the lateral spreading of the growth spiral is controlled by the slowest growing molecular step. (B) The change in step velocities in different crystallographic directions is also reflected by a different morphology of growth spirals.

growth compared to two-dimensional islands. Also, in the case of spiral growth, growth rates in different crystallographic directions change with increasing NaCl concentration resulting in more elongated growth spirals (Fig. 4B).

Similar observations have been obtained on the (001) surface of isostructural celesite. After injecting a supersaturated strontium sulfate ($S = 5.6$, no NaCl added) solution into the AFM fluid cell, two-dimensional nuclei form we observe celestite islands with an elongated morphology (Fig. 5A), which is almost identical to the morphology of barite (001) islands formed at high background electrolyte concentration (Fig. 2B). Again, the island morphology reflects the reactivity of monolayer steps in various crystallographic directions, which was also observed by Shindo *et al.* [46]. At a supersaturation of $S = 5.6$, the ratio of the island spreading rates in the [010] and [100] directions is higher compared to barite islands grown in solutions with similar ionic strength and supersaturation. The morphology of celestite (001) growth spirals is also more elongated parallel to [010] compared to barite growth spirals in pure $BaSO_4$ solution (at low ionic strength, Fig. 4B). Here again, the spiral morphology reflects the growth velocities of monolayer steps in different crystallographic directions combined with an anisotropic layer-by-layer growth in alternating $BaSO_4$ layers. Growth spirals on celestite (001) surfaces show little lateral but high vertical growth.

Dissolution: Etch Pit Formation and Monolayer Step Retreat

Similar solvent effects on monolayer step reactivity can also be obtained from *in situ* dissolution experiments. After exposing a freshly cleaved barite (001)

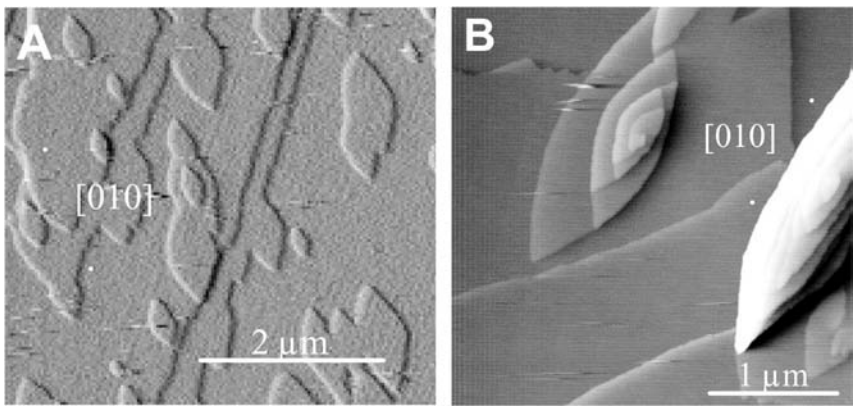

FIGURE 5 (A) AFM image of a celestite surface in 2.2 mM $SrSO_4$ solution. Two-dimensional nuclei showing a bow-shaped morphology. (B) Different stages of spiral growth.

surface to deionized water, relatively few etch pits form (upto 0.1–0.2 pits/μm^2 in 15 min, Fig. 6A). Typically, the etch pit morphology is defined by monolayer step edges parallel to ⟨120⟩ and to [010]. In consecutive molecular layers, they have opposite orientations, due to the 2_1 screw axis normal to the (001) surface. During etch pit formation, dissolution occurs via the retreat of monolayer steps. The lateral spreading rate of etch pits in pure deionized water is 0.08 ± 0.02 nm/s parallel to [010] and 0.03 ± 0.01 nm/s parallel to [100]. In high ionic strength solution (upto 1.0 M NaCl), the step reactivity and the etch pit morphology changes. The lateral spreading rate increases to 1.27 ± 0.03 nm/s parallel to [010] and 0.31 ± 0.03 nm/s parallel to [100]. As a consequence, the etch pits are more elongated parallel to [010] and bounded by curved monolayer steps (Fig. 6B). Also, the initial number of etch pits is 1.4–2.2 pits/μm^2 after 5 min, about an order of magnitude higher than in pure water.

COMPUTATIONAL RESULTS AND DISCUSSION

In order to interpret the influence of Na^+ and Cl^- in solution on the morphologies and rates of growth and dissolution of sulfate surfaces, one has to analyze the changes in the bulk solution, near-surface region, and direct interactions between

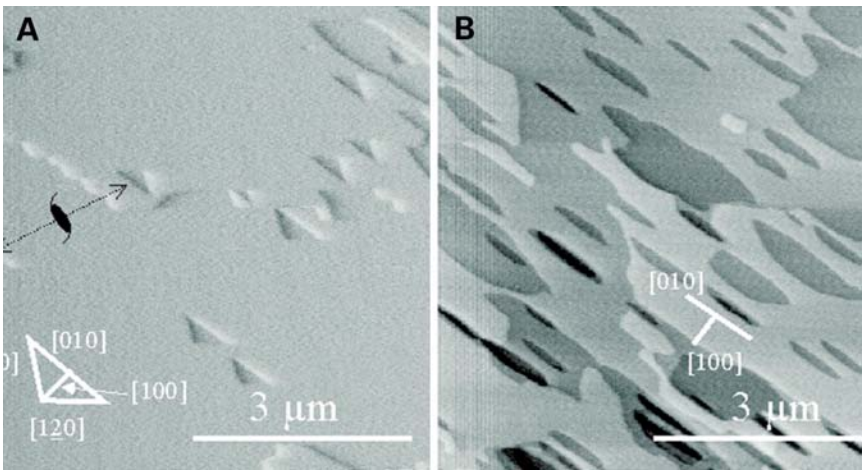

FIGURE 6 (A) AFM image of dissolution of a barite (001) surface in pure water. Triangular etch pits with a depth of half a unit cell (one monolayer) are formed on the surface. The step edges are parallel to [010], [120] and [1$\bar{2}$0]. Due to the 2_1 screw axis, triangular etch pits in consecutive atomic layers have opposite orientations. (B) In a 1.0 M NaCl solution, the etch pits become elongated with curved step edges more or less parallel to [010].

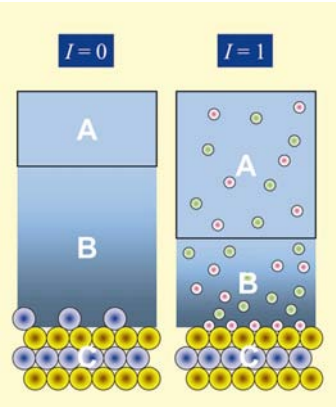

FIGURE 7 Schematic of the changes in the physico-chemical properties that are caused by adding background electrolytes to the solution that is in contact with a mineral surface. Three different regions can be distinguished and have to be considered in the analysis of growth and dissolution processes, the bulk solution (**A**), the near-surface region (**B**), and the mineral surface (**C**). In **A**, the increase in ionic strength causes changes in the activity coefficients. These effects were minimized by adjusting the concentrations of the Ba^{2+} and SO_4^{2-} ions such that their respective activity is the same in the ion-poor and ion-rich solution. The ionic strength reduces the thickness of the diffusion layer (**B**, indicated in the figure by the color change away from the surface) and the interfacial free energy in the near-surface region. Increasing the background electrolyte concentration leads to a decrease in surface and step energies (**C**) by substituting divalent surface ions by monovalent electrolyte ions.

the background electrolyte ions and the surface (Fig. 7). Since most insight can be gained from molecular simulations to resolve the mechanisms of the latter processes, we will focus on these surface processes in this study.

Dissolution

When we try to develop a picture of these etch pits from a molecular point of view of a pure $BaSO_4$ (001) surface, we obtain an etch pit as shown in Fig. 8. Figure 8 shows an etch pit that is bounded by step directions as in the experimental AFM image shown in Fig. 6. The ⟨120⟩ step directions are bounded by periodic bond chains (alternating Ba^{2+} and SO_4^{2-} ions) with no dipole moment perpendicular to the step, both first indications for a relative stable step. In contrast, the third step direction $\|\vec{b}$ would be either bounded by SO_4^{2-} or Ba^{2+} ions, resulting in a dipole moment perpendicular to the step. Such a step is energetically unfavorable, as can be calculated by the step energy. Due to the periodic boundary conditions applied in our calculations, we have to average the step energy for the SO_4^{2-} and Ba^{2+} terminated case as shown in Fig. 9A and obtain a relatively high step energy of 1.33 eV/Å (compared to 0.31 eV/Å for the PBC-like steps ‖[120]). In addition, a polar step is more likely to be attacked by water molecules from the solution due

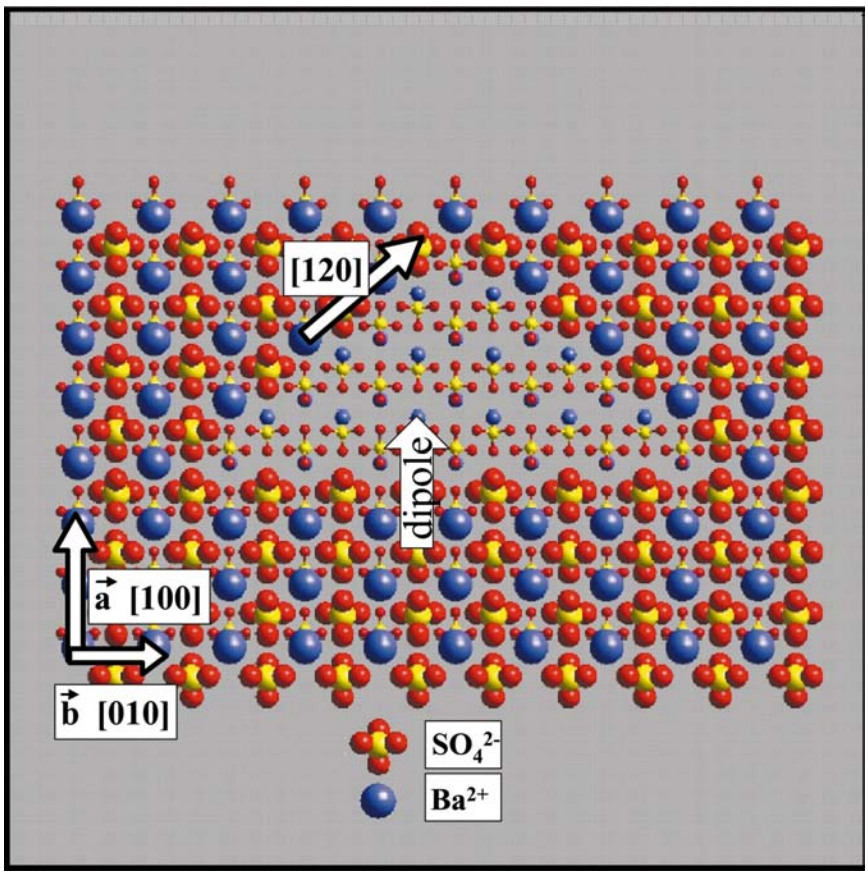

FIGURE 8 Model of an etch pit on the barite (001) surface. While there are alternating Ba^{2+} and SO_4^{2-} ions along the ⟨120⟩ directions which causes electrostatically neutral steps, straight steps along [010] consist of either Ba^{2+} or SO_4^{2-} (shown in the figure) ions. Thus, there is a strongly positively or negatively charged step (in this case negatively charged). This causes a dipole moment perpendicular to the step which is an indication for unstable step termination (atoms in the uppermost surface sublayer are represented by larger balls than in layers underneath).

to its local charge. One way to solve the problem of a local dipole moment is to "construct" a jagged edge as shown in Fig. 9B that would represent an etch pit as in Fig. 10. Figure 9A can be understood as if half of the cations are moved from the upper step edge to the lower one. The visual inspection of this figure already conveys us that there is no dipole moment perpendicular to the step any more. Therefore, the step energy (in vacuum) decreases to 0.63 eV/Å in the unrelaxed case and 0.50 eV/Å for the case where the step atoms are allowed to relax. If we stay in our framework of an etch pit that would just consist of a $BaSO_4$ surface,

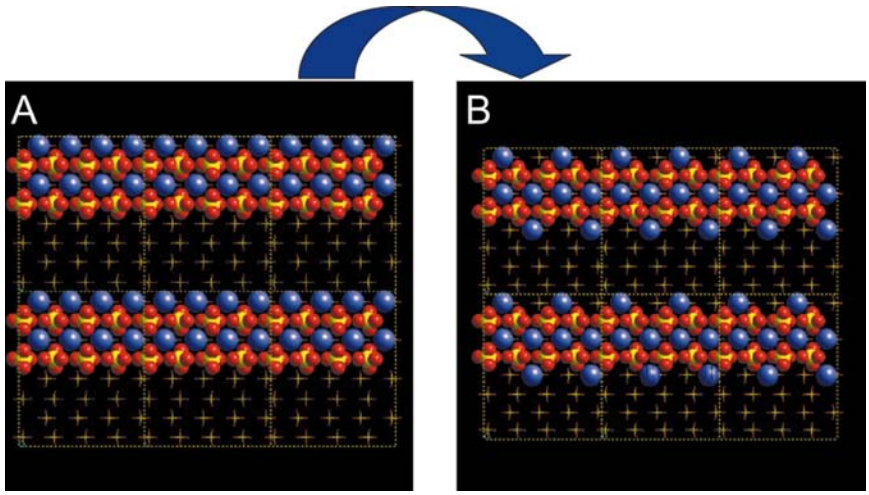

FIGURE 9 The step energy of the polar steps in (A) can be calculated using two-dimensional periodic boundary conditions. Six (3 × 2) surface unit cells are shown. The step energy is 1.33 eV/Å. (B) By moving every other Ba^{2+} ion from the top to the bottom row, the dipole moment perpendicular to the step vanishes, and the step energy reduces to 0.63 eV/Å in the unrelaxed case and 0.50 eV/Å in the relaxed case.

such a step has a high density of kink sites (1.8 kink sites/nm) which makes it more likely for hydration and, thus, for dissolution to occur (Fig. 10).

The next question is how the situation changes once the solution in contact with the etch pit contains a background electrolyte, or more strictly speaking, monovalent background electrolyte ions. We have calculated this case for a solution containing Na^+ and Cl^- ions. The case for an idealized and temporary (see below) Na^+ termination is shown in Fig. 11. Each Ba^{2+} is replaced by two Na^+ ions and the result is a dipole- and kink-free step. Interestingly, this step is less stable in vacuum (by 0.24 eV/Å) due to the Na–Na repulsion and the stronger affinity of Ba^{2+} for SO_4^{2-} than of Na^+. However, since the two-fold charge causes the hydration energy of Ba^{2+} in solution to be of the order of three times higher than the one of Na^+ (13.64 vs. 4.27 eV, [39]), the loss in hydration energy is more than compensated and the net gain is 0.17 eV/Å. Thus, the final step energy of 0.33 eV/Å is on the order of the step energy of the [120] steps. The energy budget of the adsorption of Na^+ or Cl^- to the PBC-like [120] step is much less favorable, such that we can conclude that the adsorption of monovalent background ions leads to steps that would be polar without the background electrolytes (Fig. 12). Thus, the increased relative stability of steps parallel [010] with respect to ⟨120⟩ is due to the formation of PBC-like $-Na-SO_4-Na-SO_4-$ or $-Cl-Ba-Cl-Ba-$ chains along the step, which are less polar (and hence more stable) than terraces

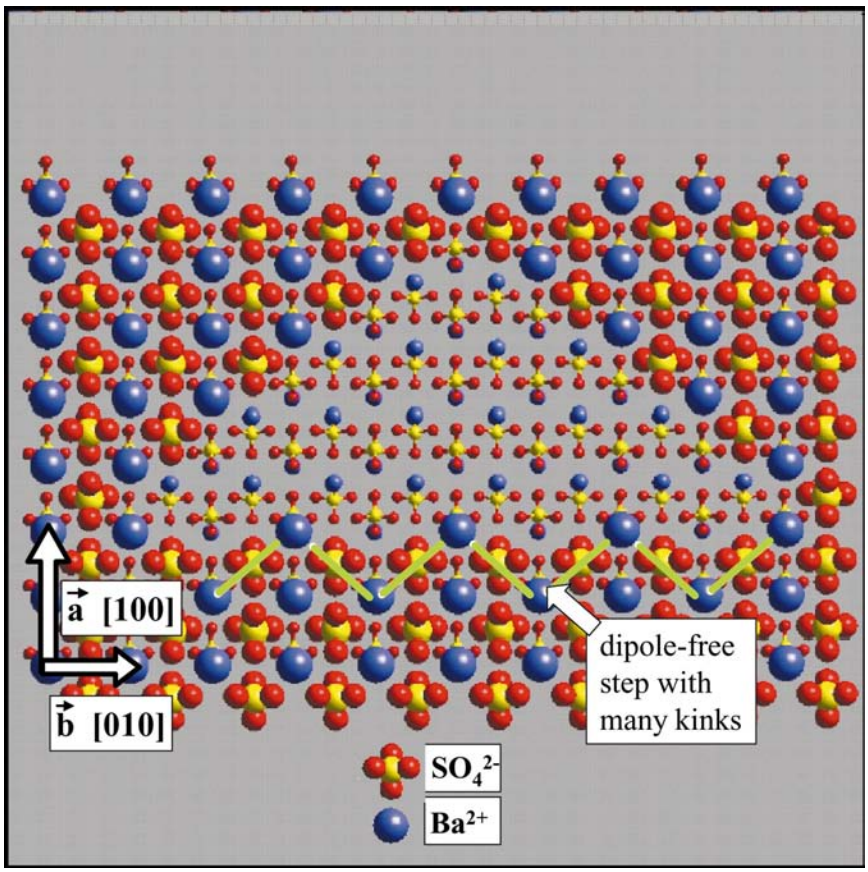

FIGURE 10 The setup in Fig. 9 creates a large number of kink sites along the [010] step direction which makes this step still significantly less favorable than steps ∥ ⟨120⟩ in pure water. Therefore, these steps do not occur in solutions with low ionic strength.

bounded by either SO_4^{2-} or Ba^{2+}. It has to be noted that the described adsorption pattern is not a static termination of the step but rather a temporary picture. The decoration of a polar step with Na^+ will always be incomplete such that dissolution progresses for undersaturated $BaSO_4$ solutions concurrent with the formation of thermodynamic equilibrium conditions between Na^+ and Ba^{2+} on step sites or between Cl^- and SO_4^{2-}. In addition, even though the adsorption of Na^+ (Cl^-) to polar steps is more favorable than the adsorption of Ba^{2+} (SO_4^{2-}), the divalent ions are energetically downhill on lattice sites of flat terraces or in the bulk.

We have also compared the adsorption of one SO_4^{2-} or two Cl^- with the adsorption of H_2-$HEDP^{2-}$ to the same steps. A sulfate ion in the "jagged step"

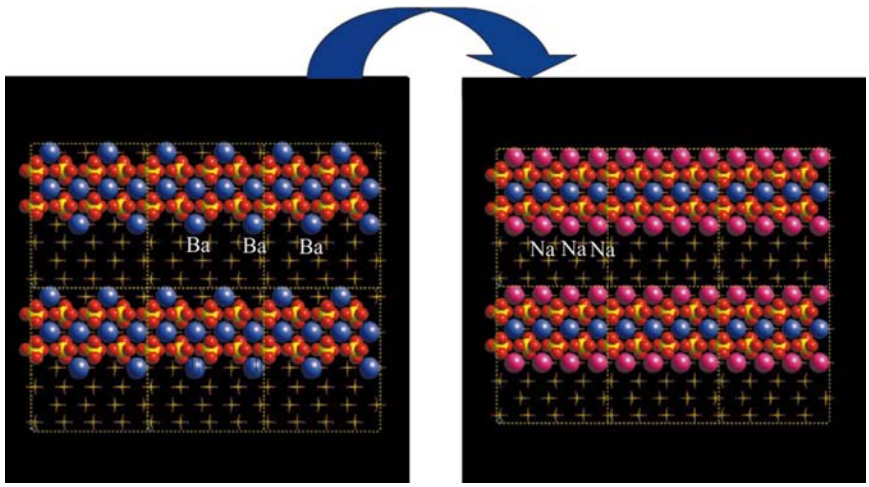

FIGURE 11 More favorable is a step termination with a row of Na^+ ions occupying every lattice site along the step compared to Ba^{2+} occupying every other site. The energy budget of such a theoretical substitution is derived in the text.

picture in Fig. 13A can either be replaced by two chloride ions or one H_2-$HEDP^{2-}$ ion (Fig. 13B). Where substitution of SO_4^{2-} is still a competitive process, the adsorption of H_2-$HEDP^{2-}$ to either [100] or [010] steps or the adsorption to kink sites on [120] steps is much stronger and thus irreversible. This explains why sites in the experimental images with H_2-$HEDP^{2-}$ bonded to them are pinned during step advancement [14] and no dynamic exchange can take place that leads to the formation of straight, crystallographically oriented steps. Even though concentrations that are typically used for growth inhibitors such as HEDP are in the μmol range and, thus, adsorption occurs in the form of single diphosphonate ions adsorbed to steps, the co-adsorption of H_2-$HEDP^{2-}$ to neighboring sites stabilizes such an adsorption site even more due to the formation of hydrogen bonds between neighboring diphosphonate ions.

The mechanism of decorating polar steps with background electrolyte ions is an explanation for the different morphologies of etch pits in solutions with and without background electrolytes. The next question to be answered is about the influence the background ions on sulfate surfaces have on the dissolution rate. We start our considerations with an "etch pit nucleus" that is bounded by steps that are parallel to PBCs (Fig. 14A). In distilled water, the first ion to be dissolved would most likely be a Ba^{2+} ion (Fig. 14B) because the binding energies of Ba^{2+} and SO_4^{2-} to the lattice are comparable, but the hydration energy of Ba^{2+} in water (13.64 eV) is significantly higher than the one for SO_4^{2-} (9.73 eV using an approximation of the Born equation of hydration, 10.58 eV using a quantum

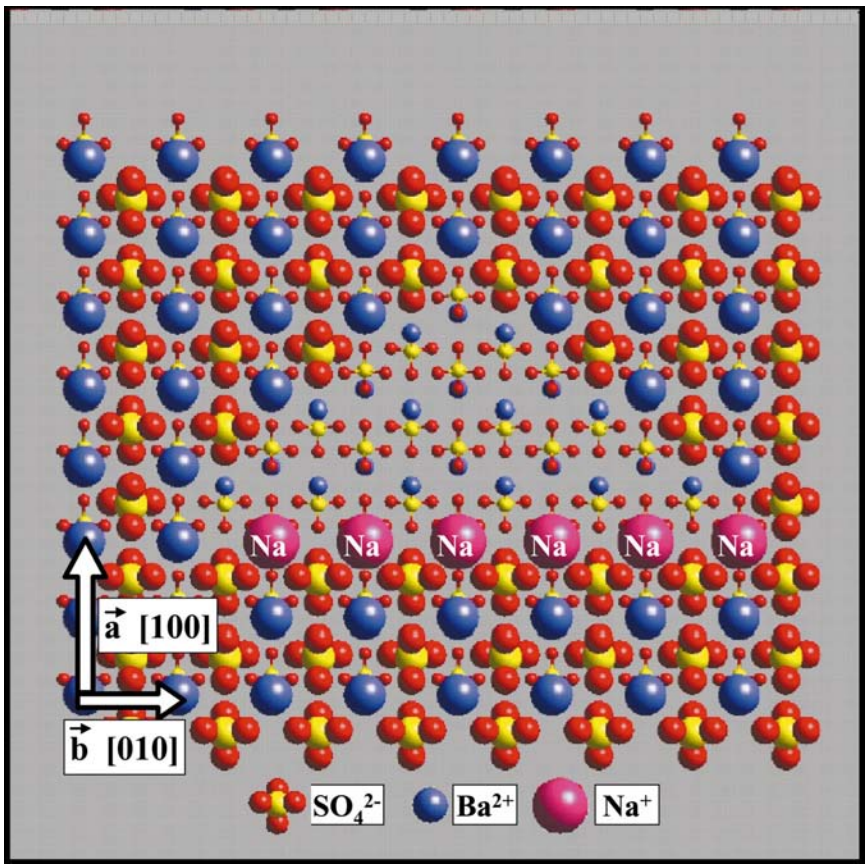

FIGURE 12 Etch pit with no background electrolyte ions along the PBC-like ⟨120⟩ steps and Na^+ termination along [010]. Similarly, one molecular row further down in the [100] direction, there would be a –Cl–Ba–Cl–Ba–Cl–chain. With this setup, all three steps have comparable step energies which nicely explains the shape of triangular etch pits found in the experimental images (e.g. Fig. 6).

mechanical approach and applying the PCM theory incorporated in the program package GAUSSIAN98, [41]). This process leaves behind a double kink site with a local charge of -2. This intermediate state is energetically uphill and therefore the rate limiting factor for the initiation of further dissolution. The solvation of cation is followed by the dissolution of a neighboring sulfate ion, which is a fast step compared to the initial dissolution (Fig. 14C). In solutions with high concentrations of background electrolytes, the unfavorable state in Fig. 14B is avoided by substituting the Ba^{2+} by a Na^+ ion, leaving no kink and a local charge of just -1 (Fig. 14D). Consecutively, a sulfate ion can be replaced by a chloride ion (Fig. 14E) and the result is a neutral substitution with relatively low activation

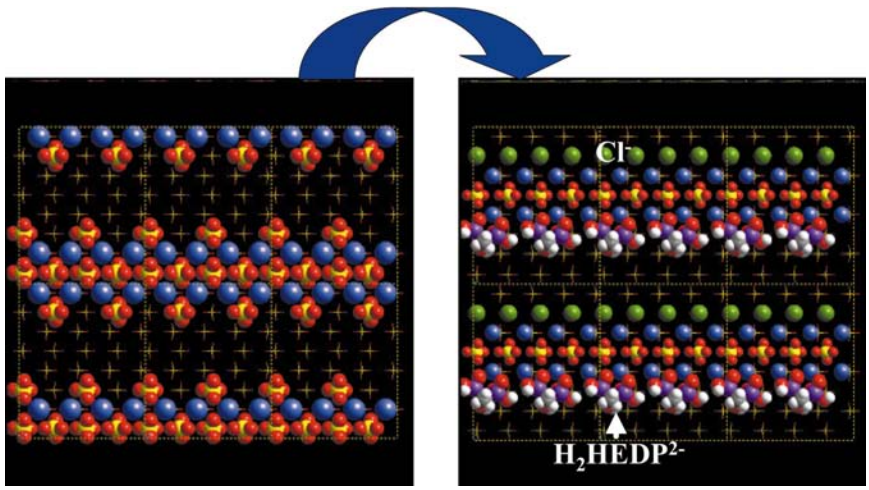

FIGURE 13 (A) Two-dimensional periodic model of a "jagged" dipole-free step, bounded by sulfate molecules. (B) The step energy can be reduced by replacing one sulfate ion by two chloride ions (green balls) along the step. Further stabilization is obtained if a sulfate ion is replaced by a H_2-$HEDP^{2-}$ ion. The high adsorption energy is caused by strong bonds between the phosphonate groups and Ba^{2+} ions along the step. If an HEDP chain is formed as shown in the figure, further stabilization is caused by hydrogen bonds between the HEDP molecules.

energies of any of the intermediate dissolution steps. This process contributes to the increased dissolution rates in solutions with a high ionic strength, in addition to the lowered interfacial free energy (strictly speaking, this mechanism also contributes to the interfacial free energy) in the near-surface region and the reduced activity coefficient in the bulk solution. This theoretical consideration of the temporary substitution of a divalent ion from the structure by a monovalent ion from solution suggests that the growth and dissolution velocity is strongly influenced by the valency of the background electrolyte ions and, via the ion exchange energy (e.g. $Ba^{2+} \leftrightarrow Na^{+}$, $SO_4^{2-} \leftrightarrow Cl^{-}$) by their atom types, as further experimental studies will have to verify.

Growth

When describing the important features of crystal growth, the key issue is to find the rate limiting steps, that is the "bottle necks" through which crystal growth has to go before more favorable adsorption events can follow. Once this rate-limiting factor is found, the next step is to find the most energetically favorable reaction path to go about this. During crystal growth of barite, sector-shaped islands (Fig. 15A) are formed with very anisotropic growth velocities (fast direction, labeled α in Fig. 15B, slow direction, labeled β, [10]). By combining the findings from

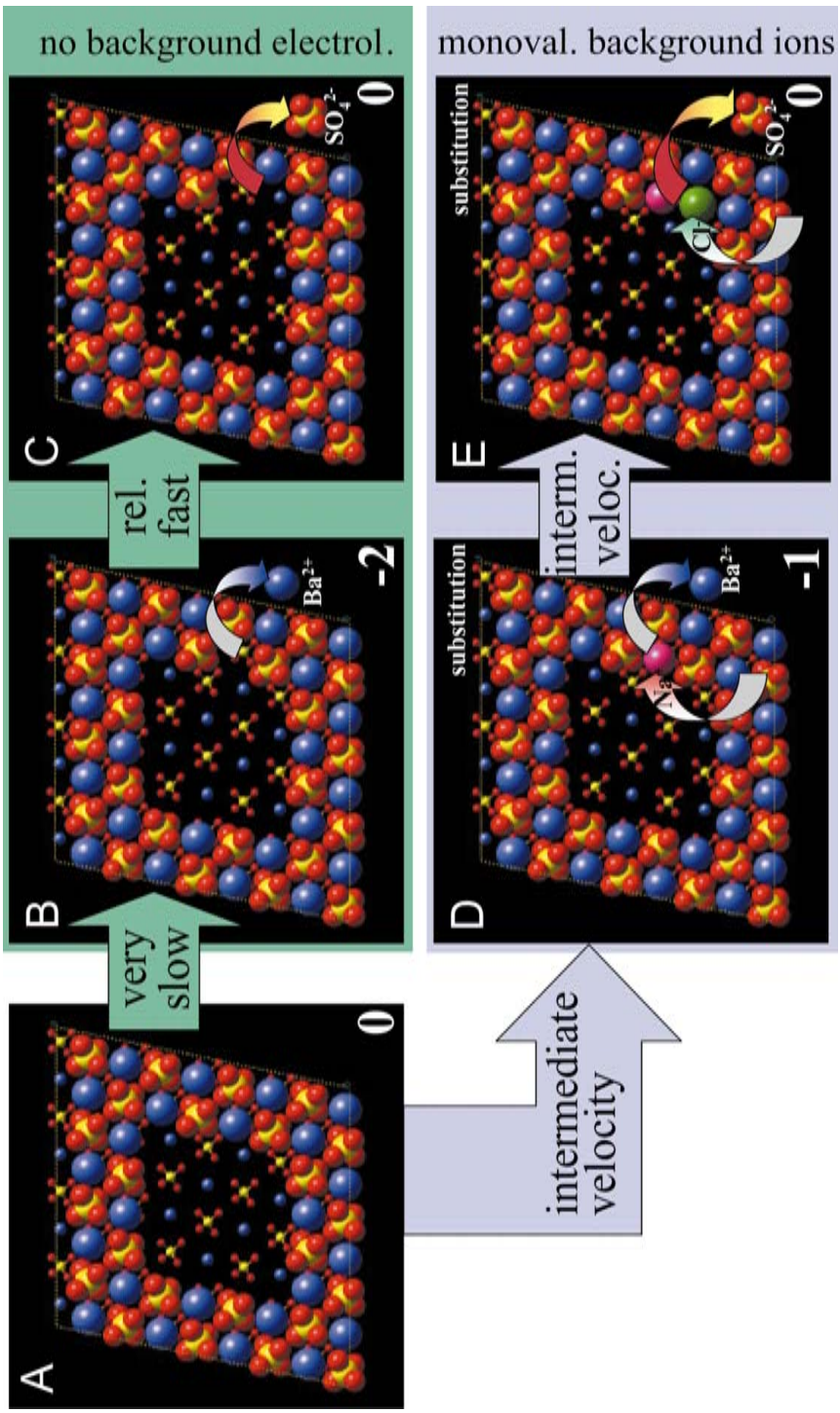

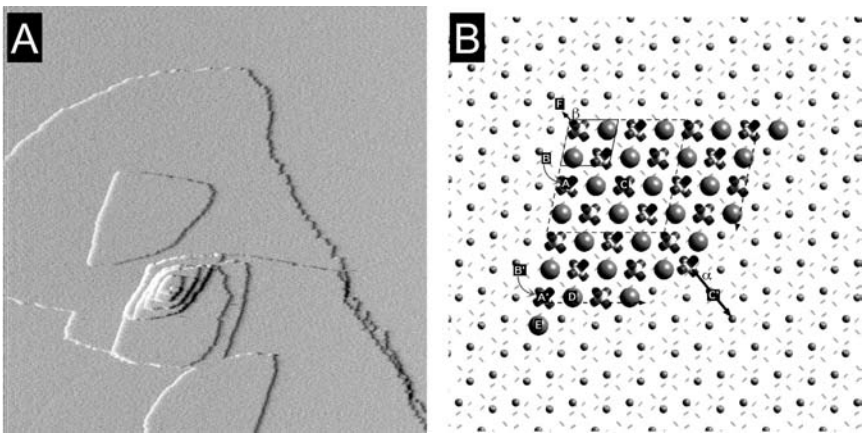

FIGURE 15 (A) Sector-shaped islands during growth on barite (001) (from [10]). (B) Molecular simulation model of the rate limiting steps during formation of a sector-shaped island shown in (A, labels are explained in the text).

AFM experiments and molecular simulations, it was found that the rate limiting step was the creation of a new growth row (at **A**, **A′**, or **E** in Fig. 15B). These rows then continue growing towards point **C′** and result in an average growth vector α. Since adsorption of ions from solution to positions **B**, **B′** and **F** is less favorable, growth in the direction of β is much slower.

Now, we need to answer the question if background electrolytes can lower the energy to create such a new growth row. Apart from changes in the diffusion layer that will be described later, the task is to compare the energetics of this first adsorption event. Let us first consider the adsorption of a Ba^{2+} cation to a potential starting island as shown in Fig. 16A. The gain in adsorption energy in vacuum to this specific site is 10.81 eV (for better graphical representation, Fig. 16 shows the unrelaxed positions of the atoms in the island and the relaxed positions of the adsorbed Ba^{2+} and Na^{+} ions). Since the newly adsorbed Ba^{2+} ion is still partly hydrated (we have calculated the remaining hydration energy on this

FIGURE 14 Schematic of barite (001) surface dissolution in pure water and in the presence of a monovalent background electrolyte solution. (A) Structure of a (theoretical) etch pit "nucleus" bound by PBCs $\|\langle 120\rangle$. (B) The dissolution of a Ba^{2+} and thus the formation of a double kink is unfavorable, because a two-fold negative site is created. This is the rate-limiting step of dissolution. (C) The consecutive step of dissolving a neighboring sulfate ion is exothermic and not rate limiting. (D) The initial dissolution step can be mediated by the substitution of Ba^{2+} by Na^{+} which makes dissolution less rate limiting than scenario (B). Even though the following substitution of a sulfate by a chloride ion is less favorable than the sulfate dissolution in (C), it is also energetically downhill and, thus, not rate limiting.

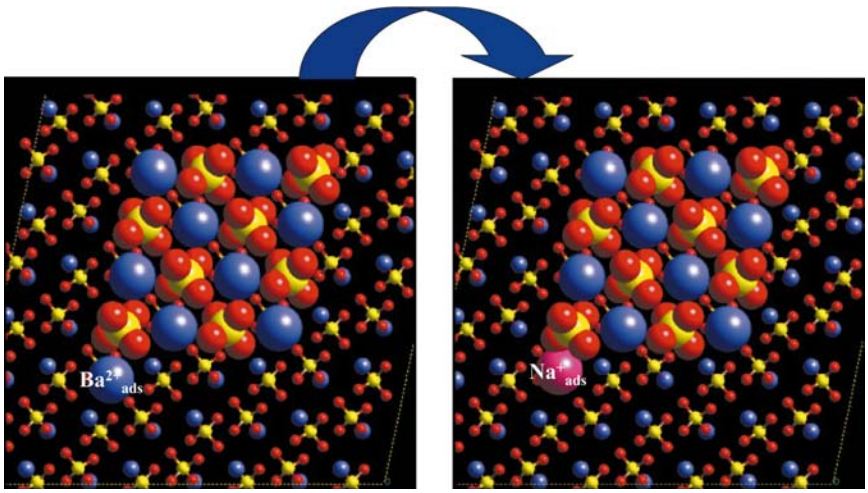

FIGURE 16 (A) In pure $BaSO_4$, the rate limiting step is the initial formation of a new growth row because the attachment of Ba^{2+} is slightly exothermic (see text for calculation of attachment energy). The formation of a temporary kink site by a Na^+ ion is energetically more favorable.

particular site to be close to 20% of the hydration energy in bulk water), the loss in hydration energy is 80% of the hydration energy of the dissolved species. Thus, the total adsorption energy in water is $-10.81 - (0.8 \times 13.64\,\text{eV}) = -0.10\,\text{eV}$. Note that these calculations have an error of at least $\pm 0.1-0.2\,\text{eV}$. Therefore, in this case, one cannot be sure if this adsorption step is exothermic or endothermic. The respective calculation for the Na^+ adsorption is $-4.94 - (0.8 \times 4.27\,\text{eV}) = -1.52\,\text{eV}$. Thus the weaker adsorption of Na^+ in vacuum is more than compensated by the much smaller loss in hydration energy. This is mainly caused by the fact that adsorption is roughly proportional to the charge of the ion but hydration is approximately proportional to the square of the charge (for equal ionic radii). Thus, we can conclude that Na^+ ions in solution can create a new row by adsorbing a "trial ion" to the preexisting island. Even though the adsorption of the next sulfate ion in such a row is less favorable in the case of Na^+ than for Ba^{2+}, in both the cases, continuation of growth is energetically downhill and thus, no growth limiting factor. It is interesting to note that the continuous growth is in favor of the incorporation Ba^{2+} rather than Na^+ and also, the substitution of the "trial adsorption site" with Na^+ by Ba^{2+} is energetically downhill. This can be explained in the following way: adsorption in vacuum is stronger than the first adsorption to the preexisting island for both cases, Na^+ ($-8.39\,\text{eV}$) and Ba^{2+} ($-16.83\,\text{eV}$) because an additional bond is formed to the neighboring sulfate ion. The gain in hydration energy during dissolution is also greater because at such a corner site, the respective ion is less exposed to the solution such that only about

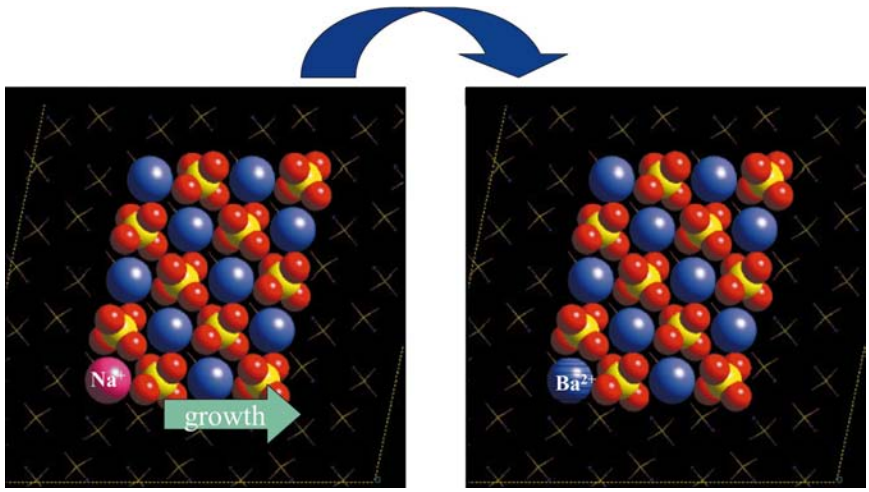

FIGURE 17 After the continuous growth of a $BaSO_4$ row (A), energy can be gained by substituting the first Na^+ ion in the row by a Ba^{2+} ion (B).

15% of the bulk water hydration is left. Therefore, we can calculate the energy balance for the substitution of Na^+ by Ba^{2+} in Fig. 17 to be:

$$\begin{aligned}\Delta E_{\text{subs}} &= -[-8.39_{\text{Na}_{\text{ads}}} + 0.85 \times 4.27_{\text{Na}_{\text{hyd}}}]\text{eV} + [-16.83_{\text{Ba}_{\text{ads}}} + 0.85 \\ &\quad \times 13.64_{\text{Ba}_{\text{hyd}}}]\text{eV} \\ &= -0.48\,\text{eV}\end{aligned}$$

This shows us that the Na^+ serves the purpose of creating a temporary adsorption site that helps to form a new step and gets substituted, which could be described as a healing effect of the crystal during continuous growth. This finding is in agreement with the fact that a Na^+ ion does not fit well into the barite structure, for reasons of both size and charge neutrality. This is already a hint from bulk crystallographic results that Na^+ or Cl^- ions in growing rows that served to create the initial kink site will subsequently be substituted by Ba^{2+} or SO_4^{2-} to complete the barite structure during growth.

Figure 18 shows the most likely structure of HEDP adsorption. One of the phosphonate groups binds to the Ba^{2+} ions at a kink site and inhibits the continuous growth of that particular $BaSO_4$ growth row. Since the binding energy of the H_2-$HEDP^{2-}$ to this kink site is much stronger than the binding energy of a sulfate ion to this site, growth is permanently inhibited unless the H_2-$HEDP^{2-}$ gets overgrown by further growth.

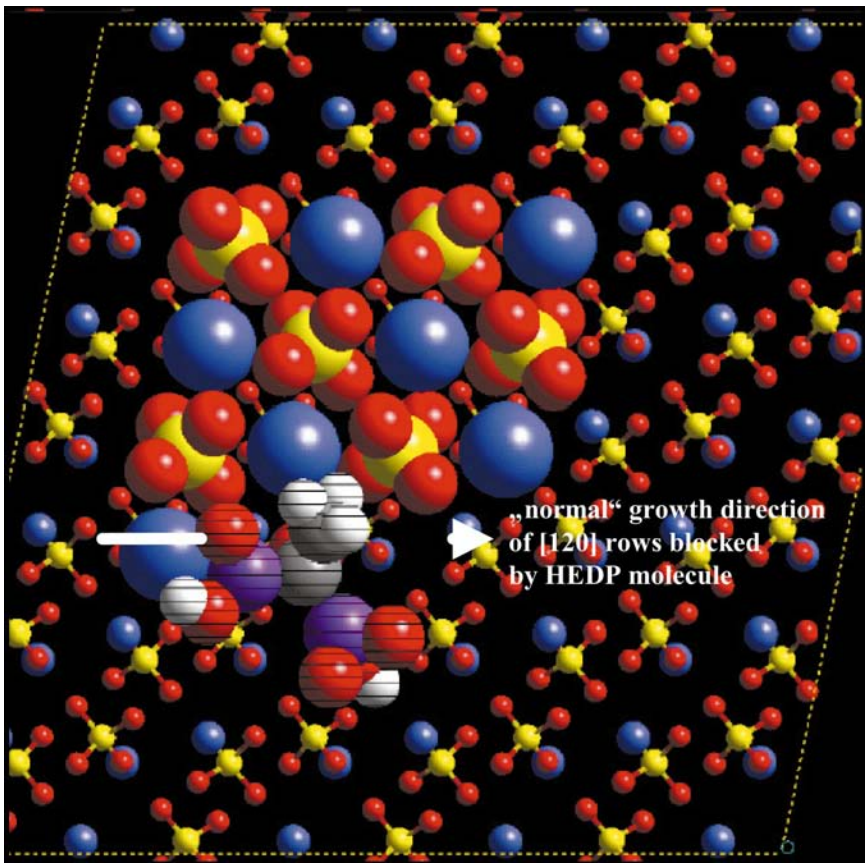

FIGURE 18 Kink blocking mechanism by H_2-$HEDP^{2-}$.

Effects of the Background Electrolyte in the Bulk Solution

The main influence of increasing the ionic strength is due to the lowering of the activity coefficients of dissolved species. Solution complexation models [38] clearly show that the presence of NaCl in the solution decreases the mean activity coefficients of Ba^{2+} and SO_4^{2-} and hence increases the solubility of barite. This may be partly responsible for the increased dissolution rate of barite in saline solutions compared to pure water.

In the experiments on barite growth, the addition of NaCl reduces the activity coefficients of Ba^{2+} and SO_4^{2-}. This effect was compensated by increasing the concentration of these ions in solution such that the activities of *free* Ba^{2+} and SO_4^{2-} ions (and hence the supersaturation) remained approximately constant. Nevertheless, the growth rate still markedly increased in the presence of NaCl

(Fig. 3). This observation, together with the morphological changes, is an experimental hint that factors such as the adsorption energies on different surface sites as described above control the growth and dissolution rates.

Effects of the Background Electrolyte in the Near-surface Region and at the Interface

He *et al.* [47] have found from homogeneous nucleation experiments that with increasing ionic strength, the interfacial energy between the solid surface and the fluid decreases.

Both, dissolution and growth are affected by a reduced interfacial energy. Two-dimensional etch pit formation during dissolution is a spontaneous process without thermal activation energy [48,49]. Therefore, the driving force is the energy gain from the elastic deformation energy in the pit volume.

Risthaus *et al.* [30] describe in great detail the influence of the ionic strength on the interfacial tension, the etch pit shape, and kink density of etch pits and growth islands using a semi-macroscopic theory. In brief, an increase of the ionic strength of the solution from 0.003 to 1 leads to an increase of the kink density by a factor of approximately three. This allows polar steps to be more stable by forming kink sites that are partially saturated by monovalent background electrolyte ions as more quantitatively described above and shown, e.g. in Figs. 11 and 12.

Another effect of the ionic strength is a near-surface solution effect, especially on kinks. If we imagine the (010) step edge that consists of zigzagged ⟨120⟩ edges, which contain a high density of kink sites with highly inhomogeneous local electric fields around them as shown in Figs. 9 and 10, in both cases, the reduction of the local interfacial energy is higher than for non-polar [120] step edges that bound islands in electrolyte-poor solutions. This is because the higher ionic strength is effectively able to screen the local electric fields around kink sites. These crystallographically selective effects hold true across the isostructural series barite–celestite. If we compare a celestite island grown in a NaCl-poor solution, we observe similar shape, growth velocities and velocity ratio of both directions in comparison to barite islands from a supersaturated solution with a high salinity.

One possible explanation for different growth morphologies of barite and celestite at low ionic strength and similar morphologies at higher ionic strength is the interfacial energy of both minerals in different solutions. He *et al.* [47] found that the interfacial energy of barite decreases from 93.4 mJ/m^2 (135 mJ/m^2 in Nielsen and Söhnel [50]) in less than 0.003 M NaCl to 79 mJ/m^2 in 1 M NaCl by

determining induction periods for homogeneous barium sulfate nucleation. This solution is comparable to our highest supersaturated barite solution with 0.75 M NaCl. The decrease in interfacial energy of barite at high ionic strength leads to similar values to those of celestite in a NaCl free supersaturated solution (85 mJ/m^2 [50]). This may indicate that similar values for the interfacial tension may be an important factor controlling the growth morphologies of different but isostructural minerals.

From all the described processes at the mineral–water interface and directly on the surface, which are influenced by species in solution, it becomes clear that a combination of mechanisms can change the morphology and kinetics of the formation of surface features. Due to the complexity of these processes, it is not always a straightforward task to determine which ions in solution are responsible for what process on the surface. Thus, it is not surprising that the morphology of deep etch pits that we observed on a celestite surface in a 1 M NaCl solution is similar to the deep etch pits on barite, that Wang *et al.* [17] observed in 0.18 M DTPA at high pH from a 1.35 M NaOH solution. Although the etch pit morphology was attributed to the specific adsorption of DTPA molecules on step edges, it is likely that the high salinity of such a solution may also play an important role in modifying the morphology. The fact that we can reproduce similar etch pits in high background electrolyte concentrations without organic molecules shows that it is important not to neglect the ionic strength in growth and dissolution experiments.

Acknowledgments

This study was funded by the Deutsche Forschungsgemeinschaft (DFG grant PU 153/1). P.R. and U.B. are also thankful for the support by the DFG from the special research area (SFB 458).

References

[1] Blount, C.W. (1977) "Barite solubilities and thermodynamic quantities upto 300°C and 1400 bars", *Am. Mineral.* **62**, 942.
[2] Busenberg, E., Plummer, L.N. and Parker, V.B. (1984) "The solubility of strontianite ($SrCO_3$) in CO_2–H_2O solutions between 2 and 91°C, the association constants of $SrHCO_3^+$ (aq) and $SrHCO_3^0$ (aq) between 5 and 80°C, and an evaluation of the thermodynamic properties of Sr^{2+} (aq) and $SrCO_3$(cr) at 25°C and 1 atm total pressure", *Geochim. Cosmochim. Acta* **48**, 2021.
[3] Reardon, E.J. and Armstrong, D.K. (1987) "Celestite ($SrSO_4$(s)) solubility in water, seawater and NaCl solution", *Geochim. Cosmochim. Acta* **51**, 942.
[4] Hardy, J.A. and Simm, I. (1996) "Low sulfate seawater mitigates barite scale", *Oil Gas J.* **94**, 64.
[5] Todd, A.C. and Yuan, M. (1990) "Barium and strontium sulfate solid solution formation in relation to North Sea scaling problems", *SPE Prod. Engng*, 279.

[6] Dove, P.M. and Czank, C.A. (1995) "Crystal-chemical controls on the dissolution kinetics of the isostructural sulfates—celestite, anglesite, and barite", *Geochim. Cosmochim. Acta* **59**, 1907.
[7] Dove, P.M. and Platt, F.M. (1996) "Compatible real-time rates of mineral dissolution by Atomic Force Microscopy (AFM)", *Chem. Geol.* **127**, 331.
[8] Archibald, D.D., Gaber, B.P., Hopwood, J.D., Mann, S. and Boland, T. (1997) "Atomic force microscopy of synthetic barite microcrystals", *J. Cryst. Growth* **172**, 321.
[9] Pina, C.M., Bosbach, D., Prieto, M. and Putnis, A. (1998) "Microtopography of the barite (001) face during growth: AFM observations and PBC theory", *J. Cryst. Growth* **187**, 119.
[10] Pina, C.M., Becker, U., Risthaus, P., Bosbach, D. and Putnis, A. (1998) "Molecular-scale mechanisms of crystal growth in barite", *Nature* **395**, 483.
[11] Bosbach, D. (2000) "Linking molecular scale barite precipitation mechanisms with macroscopic reaction rates", In: Hellmann, R., ed, Water–Rock Interactions, Ore Deposits, and Environmental Geochemistry: A Tribute to David A. Crerar Geochemical Society special publication, in press.
[12] van der Leeden, M.C. and van Rosmalen, G.M. (1995) "Adsorption behavior of polyelectrolytes on barium sulfate crystals", *J. Colloid Interface Sci.* **171**, 142.
[13] Bosbach, D., Hall, C. and Putnis, A. (1998) "Mineral precipitation and dissolution in aqueous solution: *in situ* microscopic observations on barite (001) with Atomic Force Microscopy", *Chem. Geol.* **151**, 143.
[14] Risthaus, P., Bosbach, D., Whiting, A., Coveney, P.V. and Putnis, A. "A comparison of macrocyclic organophosphonates with HEDP and NTMP as inhibitor molecules in crystal growth experiments in porous media", J. Crystal Growth (in preparation).
[15] Putnis, A., Putnis, C.V. and Paul, J.M. (1995). "The efficiency of a DTPA-based solvent in the dissolution of barium sulfate scale deposits" SPE. 29094, presented at the SPE International Symposium on Oilfield Chemistry, February 1995, San Antonio, TX, 773–785.
[16] Dunn, K. and Yen, T.F. (1999) "Dissolution of barium sulfate scale deposits by chelating agents", *Environ. Sci. Technol.* **33**, 2821.
[17] Wang, K.S., Resch, R., Dunn, K., Shuler, P., Tang, Y.C., Koel, B.E. and Yen, T.F. (1999) "Dissolution of the barite (001) surface by the chelating agent DTPA as studied with non-contact atomic force microscopy", *Colloids Surf. A* **160**, 217.
[18] Monnin, C. and Galinier, C. (1988) "The solubility of celestite and barite in electrolyte solutions and natural waters at 258°C: a thermodynamic study", *Chem. Geol.* **71**, 283.
[19] Higgins, S.R., Jordan, G., Eggleston, C.M. and Knauss, K.G. (1998) "Dissolution kinetics of the barium sulfate (001) surface by hydrothermal atomic force microscopy", *Langmuir* **14**, 4967.
[20] Shiraki, R., Rock, P.A. and Casey, W.H. (2000) "Dissolution kinetics of calcite in 0.1 M NaCl solution at room temperature: an atomic force microscopic (AFM) study", *Aquat. Geochem.* **6**, 87.
[21] He, S., Oddo, J.E. and Tomson, M.B. (1995) "The nucleation kinetics of barium sulfate in NaCl solutions upto 6 M and 90°C", *J. Colloid Interface Sci.* **174**, 319.
[22] Christy, A.G. and Putnis, A. (1993) "The kinetics of barite dissolution and precipitation in water and sodium chloride brines at 44–85°C", *Geochim. Cosmochim. Acta* **57**, 2161.
[23] Wang, K.S., Resch, R., Dunn, K., Shuler, P., Tang, Y.C., Koel, B.E. and Yen, T.F. (2000) "Scanning force microscopy study of etch pits formed during dissolution of a barite (001) surface in CDTA and EDTA solutions", *Langmuir* **16**, 649.
[24] Parker, S.C., Titiloye, J.O. and Watson, G.W. (1993) "Molecular modeling of carbonate minerals—studies of growth and morphology", *Philos. Trans. R. Soc. Lond. A* **344**, 37.
[25] Nygren, M.A., Gay, D.H., Catlow, C.R.A., Wilson, M.P. and Rohl, A.L. (1998) "Incorporation of growth-inhibiting diphosphates into steps on the calcite cleavage plane surface", *J. Chem. Soc. Faraday T.* **94**, 3685.
[26] Gerbaud, V., Pignol, D., Loret, E., Bertrand, J.A., Berland, Y., Fontecilla-Camps, J.C., Canselier, J.P., Gabas, N. and Verdier, J.M. (2000) "Mechanism of calcite crystal growth inhibition by the N-terminal undecapeptide of lithostathine", *J. Biol. Chem.* **275**, 1057.
[27] de Leeuw, N.H. and Parker, S.C. (2000) "Modeling absorption and segregation of magnesium and cadmium ions to calcite surfaces: introducing $MgCO_3$ and $CdCO_3$ potential models", *J. Chem. Phys.* **112**, 4326.
[28] de Leeuw, N.H., Parker, S.C. and Harding, J.H. (1999) "Molecular dynamics simulation of crystal dissolution from calcite steps", *Phys. Rev. B-Condens. Matter* **60**, 13792.
[29] Wright, K., Cygan, R.T. and Slater, B. (2001) "Structure of the $(10\bar{1}4)$ surfaces of calcite, dolomite and magnesite under wet and dry conditions", *Phys. Chem. Chem. Phys.* **3**, 839.

[30] Risthaus, P., Bosbach, D., Becker, U. and Putnis, A. (2001) "Barite scale formation and dissolution at high ionic strength studied with atomic force microscopy", *Colloids Surf. A: Physicochem. Engng Aspects*, in press.
[31] Allan, N.L., Rohl, A.L., Gay, D.H., Catlow, R.A., Davey, R.J. and Mackrodt, W.C. (1993) "Calculated bulk and surface properties of sulfates", *Faraday Discuss.* **95**, 1.
[32] Redfern, S.E. and Parker, S.C. (1998) "Atomistic simulation of the effects of calcium and strontium defects on the surface structure and stability of $BaSO_4$", *J. Chem. Soc. Faraday Trans.* **94**, 1947.
[33] Rohl, A.L., Gay, D.H., Davey, R.J. and Catlow, C.R.A. (1996) "Interactions at the organic/inorganic interface: molecular modeling of the interaction between diphosphonates and the surfaces of barite crystals", *J. Am. Chem. Soc.* **118**, 642.
[34] deLeeuw, N.H. and Parker, S.C. (1997) "Atomistic simulation of the effect of molecular adsorption of water on the surface structure and energies of calcite surfaces", *J. Chem. Soc. Faraday Trans.* **93**, 467.
[35] Sayle, D.C., Catlow, C.R.A., Harding, J.H., Healy, M.J.F., Maicaneanu, S.A., Parker, S.C., Slater, B. and Watson, G.W. (2000) "Atomistic simulation methodologies for modelling the nucleation, growth and structure of interfaces", *J. Mater. Chem.* **10**, 1315.
[36] Wang, K.S., Resch, R., Koel, B.E., Shuler, P., Tang, Y.C., Chen, H.J. and Yen, T.F. (1999) "Study of the dissolution of the barium sulfate (001) surface with hydrochloric acid by atomic force microscopy", *J. Colloid Interface Sci.* **219**, 212.
[37] Seo, A. and Shindo, H. (1994) "Atomic force microscopy study of directional $SrSO_4$ (001) surface and its etching property", *Appl. Surf. Sci.* **82/83**, 475.
[38] Parkhurst, D.L. and Appelo, C.A.J. (1999). "PHREEQC for Windows—A computer program for speciation, reaction-path, 1D transport and inverse geochemical calculations".
[39] Rashin, A.A. and Honig, B. (1985) "Reevaluation of the Born model of ion hydration", *J. Phys. Chem.* **89**, 5588.
[40] Becker, U., Bosbach, D. and Pina, C. (1998). "Dynamic simulation of crystal growth at the molecular scale", International Mineralogical Association, 17th General Meeting, August 9–14, Toronto, Abstract Volume, A92.
[41] Frisch, M.J., Trucks, G.W., Schlegel, H.B., Scuseria, G.E., Robb, M.A., Cheeseman, J.R., Zakrzewski, V.G., Montgomery, J.A. Jr, Stratmann, R.E., Burant, J.C., Dapprich, S., Millam, J.M., Daniels, A.D., Kudin, K.N., Strain, M.C., Farkas, O., Tomasi, J., Barone, V., Cossi, M., Cammi, R., Mennucci, B., Pomelli, C., Adamo, C., Clifford, S., Ochterski, J., Petersson, G.A., Ayala, P.Y., Cui, Q., Morokuma, K., Malick, D.K., Rabuck, A.D., Raghavachari, K., Foresman, J.B., Cioslowski, J., Ortiz, J.V., Baboul, A.G., Stefanov, B.B., Liu, G., Liashenko, A., Piskorz, P., Komaromi, I., Gomperts, R., Martin, R.L., Fox, D.J., Keith, T., Al-Laham, M.A., Peng, C.Y., Nanayakkara, A., Gonzalez, C., Challacombe, M., Gill, P.M.W., Johnson, B., Chen, W., Wong, M.W., Andres, J.L., Gonzalez, C., Head-Gordon, M., Replogle, E.S. and Pople, J.A. (1998) "GAUSSIAN 98, Revision A.7", Gaussian, Inc., Pittsburgh PA.
[42] Miertus, S. and Tomasi, J. (1982) "Approximate evaluations of the electrostatic free energy and internal energy changes in solution processes", *Chem. Phys.* **65**, 239.
[43] Hagler, A.T., Huler, E. and Lifson, S. (1974) "Energy functions for peptides and proteins. i. derivation of a consistent force field including the hydrogen bond from the amide crystals", *J. Am. Chem. Soc.* **96**, 5319.
[44] Gale, J. (1998) GULP (General Utility Lattice Program) Imperial College/Royal Institution of Great Britain.
[45] Hartman, P. and Heijnen, W.M.M. (1983) "Growth mechanisms of a crystal-face for which more than one surface-structure is possible", *J. Cryst. Growth* **63**, 261.
[46] Shindo, H., Shitagami, K., Kondo, S. and Seo, A. (1999) "Atomic force microscopic observation of directional layer growth and dissolution on surfaces of sulfate minerals", *J. Cryst. Growth* **198/199**, 253.
[47] He, S., Oddo, J.E. and Tomson, M.B. (1995) "The nucleation kinetics of barium sulfate in NaCl solutions upto 6 M and 90°C", *J. Colloid Interface Sci.* **174**, 319.
[48] Cabrera, N. (1956) "The formation of etch pits and of oxide nuclei at dislocations", *J. Chem. Phys.* **53**, 675.
[49] Heimann, R.B. (1975) Auflösung von Kristallen (Springer, Berlin).
[50] Nielsen, A.E. and Söhnel, J. (1971) "Interfacial tensions of electrolyte crystal—aqueous solutions from nucleation data", *J. Cryst. Growth* **11**, 233.